Real-time turbulence profiling using particle filtering

Jonatan Lehtonen[a] and Tapio Helin[b]

[a]University of Helsinki, Finland
[b]LUT University, Finland

ABSTRACT

A number of experiments have demonstrated that turbulence profiles can change very rapidly. However, turbulence profiling techniques typically rely on estimating correlations from up to a few minutes of data, delivering accurate profiles at the cost of a time delay. We present a novel method for tracking the turbulence profile in real time using AO telemetry. This method can provide complementary information without requiring any additional instruments, and may provide new insights into turbulence dynamics.

Keywords: turbulence, adaptive optics, tomography, real-time, profiling, particle filter

1. INTRODUCTION

Astronomical Adaptive Optics (AO) systems refer to technology deployed on ground-based optical telescopes, improving imaging quality by providing real-time compensation of disruptive optical aberrations caused by atmospheric turbulence.[1] They are poised to become mainstream in the next generation instruments and telescopes.

After the successful application on single-conjugated AO systems, current and soon-to-be designs attempt to provide correction over larger fields of view, typically on the order of tens of arcseconds to a few arcminutes.[2] The latter rely on the tomographic estimation (and subsequent correction) of the turbulence above the telescope, which is an ill-posed problem.[2,3] To this end, several measurements along different lines-of-sight are used before applying the optical correction by driving deformable mirrors with optimal opposite shapes.[4] On account of the small angles (around 1–7 arcmin) and limited computational resources, any successful solution strategy in atmospheric tomography is based on reliable statistical modeling of the turbulence, such as the *turbulence profile*.[5,6]

Several methods exist for finding the turbulence profile, which is given as a vertical distribution of the refractive index structure constant C_n^2. The most common methods are the Multi Aperture Scintillation Sensor (MASS),[7] SLOpe Detection And Ranging (SLODAR)[8,9] and SCIntillation Detection And Ranging (SCIDAR).[10,11] All of these methods rely on averaging data over a period of up to a few minutes in order to estimate correlations, either from scintillation patterns or from wavefront sensor (WFS) measurements. This produces high-quality measurements of the correlations, which can be leveraged to obtain high-resolution profiles,[12] or to recover more information about the turbulence statistics such as the outer scale[13–15] or even the power spectral density.[16] However, this averaging also presents a fundamental limitation in terms of temporal resolution, which means that the profile used as a prior for atmospheric tomography may be based on data from several minutes before.

In this paper we address the limitation in temporal resolution by proposing a novel method for tracking the turbulence profile evolution in real time using WFS measurements from the AO system. At each observation partial information of the current turbulence profile is propagated to the WFS data due to the dependence of the turbulence layer statistics on the C_n^2-profile. This dependence gives rise to a likelihood probability distribution of observed data given the state of the turbulence profile. Here, we propose the use of a particle filtering algorithm that utilizes such an observational model with a simple random walk model for the turbulence profile evolution.

Further author information: (Send correspondence to J.L.)
J.L.: E-mail: jonatan.lehtonen@helsinki.fi
T.H.: E-mail: tapio.helin@lut.fi

To the best of our knowledge, there is no experimental data or method available describing the dynamics of the C_n^2-profile beyond the time resolution achieved by SLODAR or SCIDAR measurements. Therefore, our method has not only the potential to improve tomographic reconstruction or point spread function estimation in terms of more accurate C_n^2-profiles, but it can also reveal new interesting information of atmospheric turbulence dynamics when applied to real data. In this work, we demonstrate the performance of a particle filtering approach using simulated time-dependent profiles with temporal resolution of a tenth of a second. The averages of these profiles over longer time periods agree with real measurements obtained with Stereo-SCIDAR at Paranal.[12] However, since there is no information on how strong the dynamics might be, the role of our simulated profile is merely to indicate what kind of fast changes or oscillations in the C_n^2-profile can be tracked.

We begin in Section 2 by describing how the turbulence profile relates to the Shack–Hartmann wavefront sensor measurements obtained by an AO system, and present a simplified model for how the turbulence profile evolves in time; these are crucial building blocks for developing a filtering algorithm. In Section 3 we give a general description of filtering methods, and present the specific particle filtering algorithm we have used. Section 4 describes our numerical simulations of an AO system, complete with simulated boiling and a time-dependent turbulence profile based on real SCIDAR profiles. The results obtained from applying our algorithm to the simulated data are presented in Section 5, followed by a discussion of the results and future prospects in Section 6.

2. MODELING TURBULENCE AND ITS EVOLUTION

Developing an algorithm for tracking changes in the turbulence profile in real time requires a good understanding of how WFS measurements depend on the profile, as well as a model for how the profile evolves in time. We begin with the former as it is readily available from atmospheric tomography.

We assume that the atmospheric turbulence can be well-represented by K two-dimensional layers, which can be discretized to obtain vectors $\boldsymbol{\phi} = (\boldsymbol{\phi}_1, \ldots, \boldsymbol{\phi}_K)$ representing the phase fluctuations for each layer. We further assume that these layers are independent, isotropic and stationary, and that they follow the von Kármán model of turbulence. Using this model we can derive a covariance matrix $\boldsymbol{C}_k$ for each layer, and consider $\boldsymbol{\phi}$ as a Gaussian vector such that $\boldsymbol{\phi} \sim \mathcal{N}(0, \boldsymbol{C}(\boldsymbol{\rho}))$ *, where

$$\boldsymbol{C}(\boldsymbol{\rho}) = \begin{pmatrix} \rho_1 \boldsymbol{C}_1 & \ldots & 0 \\ \vdots & \ddots & \vdots \\ 0 & \ldots & \rho_K \boldsymbol{C}_K \end{pmatrix}. \tag{1}$$

Above, the covariance matrices $\boldsymbol{C}_k$ for each layer are given by the von Kármán model and $\boldsymbol{\rho} = (\rho_1, \ldots, \rho_K)^{\mathrm{T}}$ is the turbulence profile which gives the turbulence strength for each layer. Given this layered model for atmospheric turbulence, we can then describe the measurement model for Shack–Hartmann WFSs by

$$\boldsymbol{s} = \boldsymbol{A}\boldsymbol{\phi} + \boldsymbol{\varepsilon}, \quad \boldsymbol{\phi} \sim \mathcal{N}(0, \boldsymbol{C}(\boldsymbol{\rho})), \tag{2}$$

where $\boldsymbol{s}$ is a vector of WFS measurements, $\boldsymbol{A}$ is the atmospheric tomography operator, and $\boldsymbol{\varepsilon} \sim \mathcal{N}(0, \boldsymbol{\Gamma})$ is the photon noise of the WFS, which we model as Gaussian white noise with covariance matrix $\boldsymbol{\Gamma}$. Note that since our model for the turbulence $\boldsymbol{\phi}$ depends on the turbulence profile $\boldsymbol{\rho}$, this measurement model gives us an implicit connection between the turbulence profile and the WFS measurements $\boldsymbol{s}$.

It is important to note that while (2) does provide a link between the turbulence profile and WFS measurements, data from a single WFS does not in fact carry significant information about the turbulence profile, as there is no way to distinguish between the different layers. Instead, we will need measurements from multiple wavefront sensors along different lines-of-sight, similar to the measurement setup used in SLODAR, where correlations of measurements from several WFSs are used to recover the turbulence profile.[8,9] However, while in SLODAR these correlations are modeled explicitly and estimated over long periods of time, our method will only require the implicit connection between $\boldsymbol{\rho}$ and $\boldsymbol{s}$ provided by the model in (2).

---

*The notation $\boldsymbol{x} \sim \mathcal{N}(\boldsymbol{m}, \boldsymbol{C})$ indicates that the random vector $\boldsymbol{x}$ follows the multivariate normal distribution with mean $\boldsymbol{m}$ and covariance matrix $\boldsymbol{C}$.
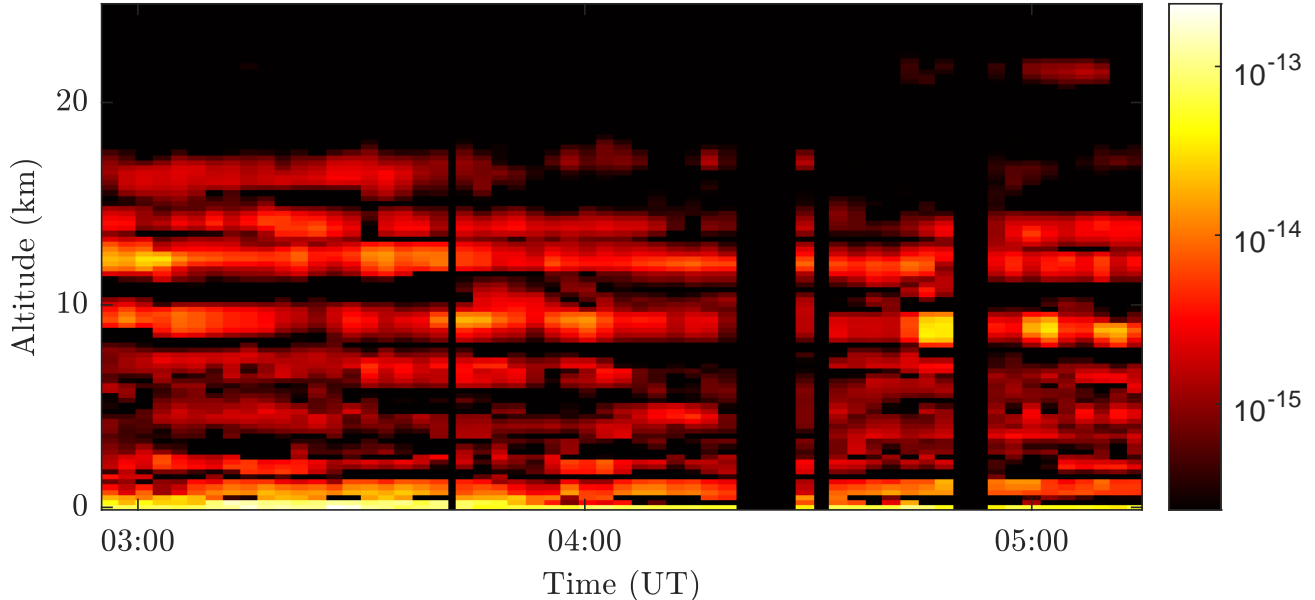
Figure 1. Turbulence profiles obtained with Stereo-SCIDAR at Paranal on the night beginning 8th March 2017, with an average temporal resolution of 140 s; the gaps in the data are due to missing profiles.[12] As can be seen from the image, the profiles can undergo rapid changes where individual layer strengths change by almost an order of magnitude between consecutive profiles. This is particularly evident in the last nine profiles on the right, where the strength of the layer at 9 km oscillates several times, with the peaks being up to ten times stronger than the lows.

As mentioned previously, we will also need a model for the temporal evolution of $\boldsymbol{\rho}$. Fig. 1 shows an example of this evolution, based on turbulence profiles obtained at Paranal with Stereo-SCIDAR. The profile can sometimes change very rapidly, with the strength of individual layers changing by an order of magnitude in a matter of minutes. However, there is no discernible pattern to these changes, as the fluctuations appear to be quite random. Since any physical model for this evolution would likely be too complicated and depend on many external variables such as wind speeds and directions, we have instead chosen to use a very simple evolution model given by

$$\boldsymbol{\rho}^{j+1} = \boldsymbol{\rho}^j + \boldsymbol{\eta}^j, \quad \boldsymbol{\eta}^j \sim \mathcal{N}(0, \boldsymbol{\Sigma}), \tag{3}$$

where the index j indicates the timestep and $\boldsymbol{\eta}^j$ is Gaussian white noise with a covariance matrix $\boldsymbol{\Sigma}$. The evolution is thus modeled as a random normally distributed change to the turbulence profile. While this model is indeed very simple, it is well-suited for filtering methods and works well in practice, as will become evident in Section 5.

3. PARTICLE FILTERING

Our goal is to track the evolution of the turbulence profile in real time based on measurements obtained from the AO system. This is an example of a so-called filtering problem, where the aim is to produce the best possible estimate of the current state of a dynamical system based on noisy measurements of that system.[17] The estimate is given as a probability distribution on the state variables, which is updated as new measurements are obtained.

Filtering problems have two key components: an evolution model for the state variables that we are interested in, and an observational model describing how the data obtained from the dynamical system depends on those variables. In statistical filtering, evolution and observation are described by conditional probability distributions: what is the probability density of the next state $\boldsymbol{\rho}^{j+1}$ given $\boldsymbol{\rho}^j$ and what is the likelihood of measurement outcome $\boldsymbol{s}^j$ given $\boldsymbol{\rho}^j$?

The evolution model given in (3) yields the distribution of $\mathbb{P}(\boldsymbol{\rho}^{j+1} \mid \boldsymbol{\rho}^j)$. However, the observational model is not implied from (2) trivially as the WFS measurements $\boldsymbol{s}^j$ are only implicitly connected to the turbulence

profile $\boldsymbol{\rho}^j$ through the prior for the atmospheric turbulence $\boldsymbol{\phi}^j$. However, by integrating over the turbulence layer variables it can be derived that

$$\mathbb{P}(\boldsymbol{s}_j|\boldsymbol{\rho}_j) \sim \mathcal{N}(0, \boldsymbol{\Gamma} + \boldsymbol{A}^{\mathrm{T}}\boldsymbol{C}(\boldsymbol{\rho}_j)\boldsymbol{A}). \tag{4}$$

Notice carefully that in the millisecond time scale we have frozen flow and, consequently, subsequent observations are not independent realizations of the distribution $\mathbb{P}(\boldsymbol{s}|\rho_j)$. However, in the following we assume that observations are made at sufficient time intervals such that the subsequent observations are not strongly correlated.

We solve the filtering problem by applying a particle filtering method known as *sequential importance resampling*.[17] The distribution of $\boldsymbol{\rho}_j$ is approximated by N "particles" $\boldsymbol{\rho}_j^{(i)}$ and associated weights $w_j^{(i)}$. Together these define a conditional probability distribution for $\boldsymbol{\rho}_j$ as a sum of weighted Delta distributions:

$$\mu_j^N = \mathbb{P}(\boldsymbol{\rho}_j|\boldsymbol{s}_{1:j}) := \sum_{i=1}^N w_j^{(i)}\delta(\boldsymbol{\rho}_j - \boldsymbol{\rho}_j^{(i)}). \tag{5}$$

In other words, the particles $\boldsymbol{\rho}_j^{(i)}$ represent possible realizations of the turbulence profile, with the weights $w_j^{(i)}$ indicating their relative probability.

We begin with N particles of equal weight, sampled uniformly from all non-negative vectors whose components sum to some initial guess of the total turbulence strength. This distribution is then updated at each timestep j as follows:

1. Draw $\boldsymbol{\rho}_j^{(i)} \sim \mu_j^N$, $i = 1, \ldots, N$, where μ_j^N is given by (5).

2. Sample new particle locations $\widehat{\boldsymbol{\rho}}_{j+1}^{(i)}$ from the evolution model given by (3): $\widehat{\boldsymbol{\rho}}_{j+1} = \boldsymbol{\rho}_j + \boldsymbol{\eta}_j$.

3. Compute $w_{j+1}^{(i)} = \mathbb{P}(\boldsymbol{s}_{j+1}|\widehat{\boldsymbol{\rho}}_{j+1}^{(i)})$ according to (4) and normalize through $w_{j+1}^{(i)} = w_{j+1}^{(i)}/\sum_{i=1}^N w_{j+1}^{(i)}$.

4. Define the new distribution as $\mu_{j+1}^N = \sum_{i=1}^N w_j^{(i)}\delta_{\boldsymbol{\rho}_j^{(i)}}$.

The so-called resampling in step 1 is done to avoid a situation where almost all particles have zero weight, as this would effectively mean having much fewer particles.

We have found that computing the weights according to (4) in step 3 above can be computationally challenging, as evaluating the probability distribution involves both multiplying a vector by the inverse of the covariance matrix and computing its determinant. Since the covariance matrix is of size $M \times M$, where M is the number of WFS measurements, the computational cost of these operations quickly becomes prohibitive. For example, two WFSs with 74×74 subapertures yield a total of 21904 measurements, and evaluating the probability distribution would take well over ten seconds per particle.

In order to overcome this issue of dimensionality, we split the WFS into 1448 square subregions ranging in size from a single subaperture to 12×12 and even 37×37 subapertures. The WFS measurements are averaged within each of these subregions, which then effectively act as larger Shack–Hartmann subapertures. This dimension reduction allows us to evaluate the probability distribution $\mathbb{P}(\boldsymbol{s}_{j+1}|\widehat{\boldsymbol{\rho}}_{j+1}^{(i)})$ in just 25 ms per particle, a reduction of nearly three orders of magnitude in computation time.

4. SIMULATING PHASE SCREENS WITH BOILING

The simulations were done using MOST, a MATLAB tool for simulating adaptive optics systems, developed by the AAO team at JKU Linz in Austria. We simulated an AO system with the following properties:

- 37 m telescope with two Shack–Hartmann WFSs, each having 74×74 subapertures; the corresponding LGSs were at an altitude of 90 km, separated by an angle of 2.5 arcminutes

- WFS photon noise level corresponding to a flux of 50 photons per subaperture per frame

- Ten discrete layers of von Kármán turbulence with the outer scale $L_0 = 25\,\text{m}$

- C_n^2-profile evolving in time based on real SCIDAR profiles, with total r_0 ranging from $18\,\text{cm}$ to $27\,\text{cm}$; this is explained in more detail below

- Wind speeds for layers ranged from $5.5\,\text{m}\,\text{s}^{-1}$ to $27.5\,\text{m}\,\text{s}^{-1}$, staying constant throughout the simulation

- The atmosphere and AO system were simulated for 10 minutes at a rate of $10\,\text{Hz}$, for a total of 6001 frames

Our aim was to model the temporal evolution of turbulence as realistically as possible. This was achieved by simulating a time-dependent C_n^2-profile based on real turbulence profiles obtained with Stereo-SCIDAR at Paranal on the night beginning 8th March 2017, shown in Fig. 1. We chose nine consecutive profiles which exhibited unusually large changes in turbulence strength. These profiles were binned from the original 100 layers down to 10 by manually selecting altitude bins which corresponded to significant features in the turbulence profiles. The total turbulence strength in each bin was assigned to a single layer, with the altitude given by the weighted average of all layers in that bin, rounded to a multiple of $250\,\text{m}$ to match existing SCIDAR profile altitudes.

Based on the binned SCIDAR profiles, we generated a time-dependent 10-layer profile, which is shown as the reference profile in Fig. 2. This profile was randomly generated to match the binned SCIDAR profiles when averaged over a corresponding time frame.[†] Since the temporal resolution of the SCIDAR data is approximately $140\,\text{s}$, the total duration of the generated profile is over 20 minutes. In our simulations we used 10 minutes of this profile, starting from the beginning of the third SCIDAR profile. This ensures that the temporal evolution of the simulated profile is fully consistent with the SCIDAR data, as it also takes into account the profiles from before and after the simulated time frame.

We also concluded that modeling the evolution of turbulence purely based on Taylor's frozen flow hypothesis[18] would be inadequate, as it is only valid on a timescale of a few seconds or less due to effects such as boiling.[19] Motivated by this, we simulated boiling phase screens using an auto-regressive method,[20] where a given percentage of each phase screen is replaced with a new phase screen sharing the same power spectral density. This causes the phase screens to change slowly while keeping the same statistics.

In Ref. 20, the authors estimated boiling rates using on-sky data from the Gemini Planet Imager, and found boiling coefficients of 0.991 to 0.996 for a $1000\,\text{Hz}$ system; this number indicates how much of the original phase screen is carried forward by frozen flow in each timestep, with the rest being replaced by a new phase screen due to boiling. We chose to simulate a boiling coefficient of 0.995, which yields a coefficient of 0.606 for our $10\,\text{Hz}$ system. The reason for using a frame rate of only $10\,\text{Hz}$ is two-fold. Firstly, it significantly cuts down the computation time for both simulations and the filter, allowing us to instead simulate over a longer time period. Secondly, as described in Section 3, using a slower frame rate gives the atmosphere more time to evolve, which means that each individual frame carries significantly more new information about the atmosphere.

5. RESULTS

In this section we present the results obtained from applying our real-time turbulence profiling method to the simulated data described in Section 4. The filtering was done using 1000 particles, which were initialized by sampling uniformly at random from profiles with total turbulence strength corresponding to a Fried parameter of $r_0 = 20\,\text{cm}$. It should be noted that the simulated profile had an initial r_0 of $21.8\,\text{cm}$, which means that our initial profiles had $15.5\,\%$ higher total C_n^2 than the simulated profile.

Fig. 2 shows the real-time turbulence strength obtained for each layer, normalized by the turbulence strength corresponding to an r_0 of $20\,\text{cm}$. Since the method described in Section 3 gives us a probability distribution for the profile, the plots in Fig. 2 include both the mean and the $95\,\%$ credible interval of the distribution. The

---

[†]The profile was generated by randomly sampling a Gaussian random field with a squared exponential covariance function. This is also how turbulence is simulated, although the chosen covariance function produces significantly smoother functions than the von Kármán turbulence model. The sampling was done with a strong prior condition to favor profiles with averages which closely match the binned SCIDAR profiles in corresponding time frames.
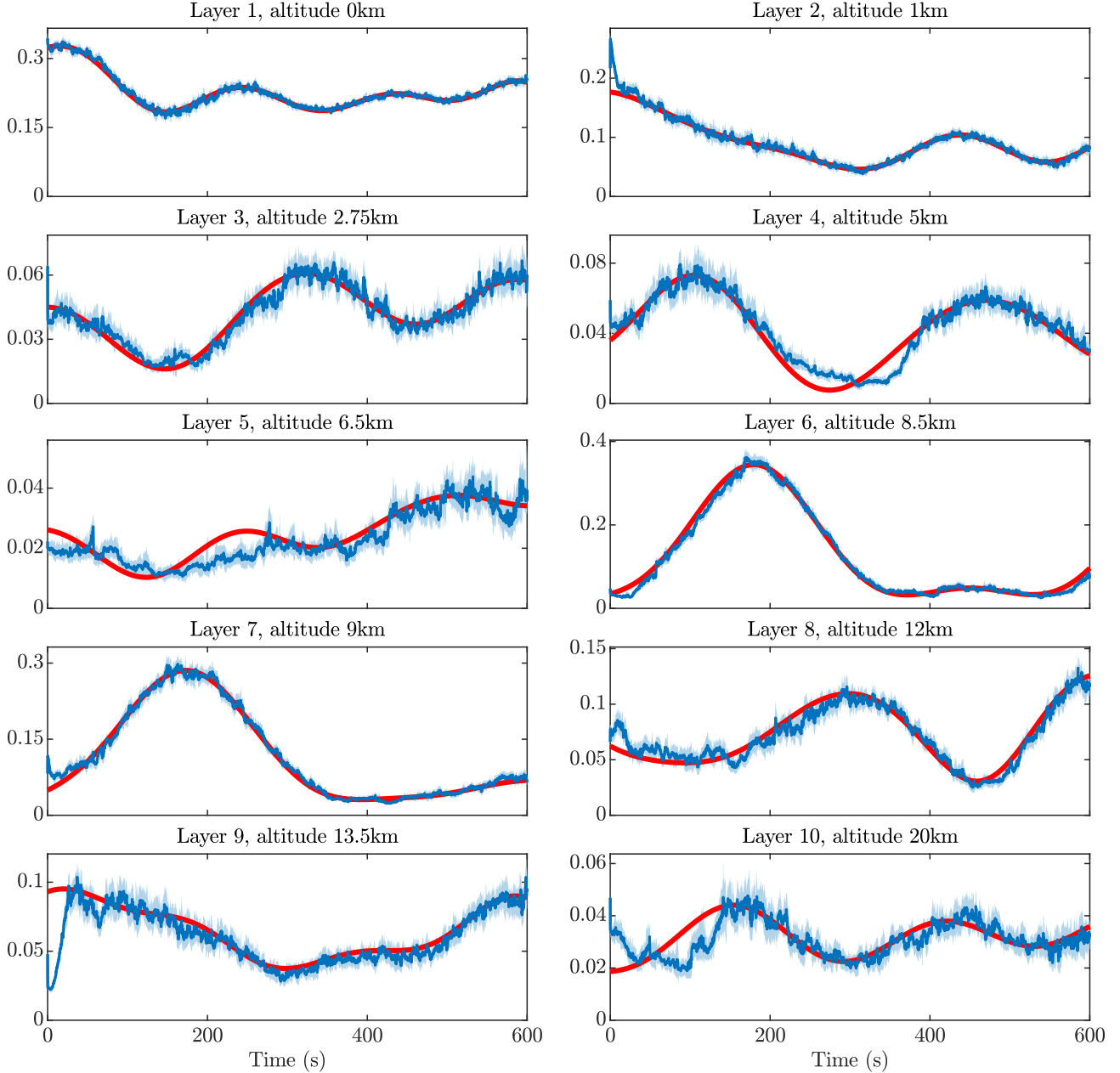
Figure 2. The particle filter was applied to the simulated data described in Section 4. This plot shows the true profile (red) and the estimate (blue), i.e. the mean of the filtering distribution at each timestep. The credible intervals which contain 95 % of the probability distribution at each timestep are also shown (light blue). The C_n^2-values on the vertical axis have been scaled by the C_n^2 corresponding to an r_0 of 20 cm to make the relative strength of each layer clearer.

estimate given by the filter may appear significantly noisier for some of the layers, but this is primarily due to the vertical axis being scaled differently for each layer, as the layer strengths differ by up to an order of magnitude.

We can see from Fig. 2 that the filter follows changes in the simulated profile quite well. There are some visible errors with layers 4 and 5, although these errors are likely due to the simultaneous rapid drop for layers 6 and 7, especially since the latter are significantly stronger. Apart from this, the only notable errors are at the start, which is to be expected given the random initialization with over 15 % higher total C_n^2 than in the simulated profile.
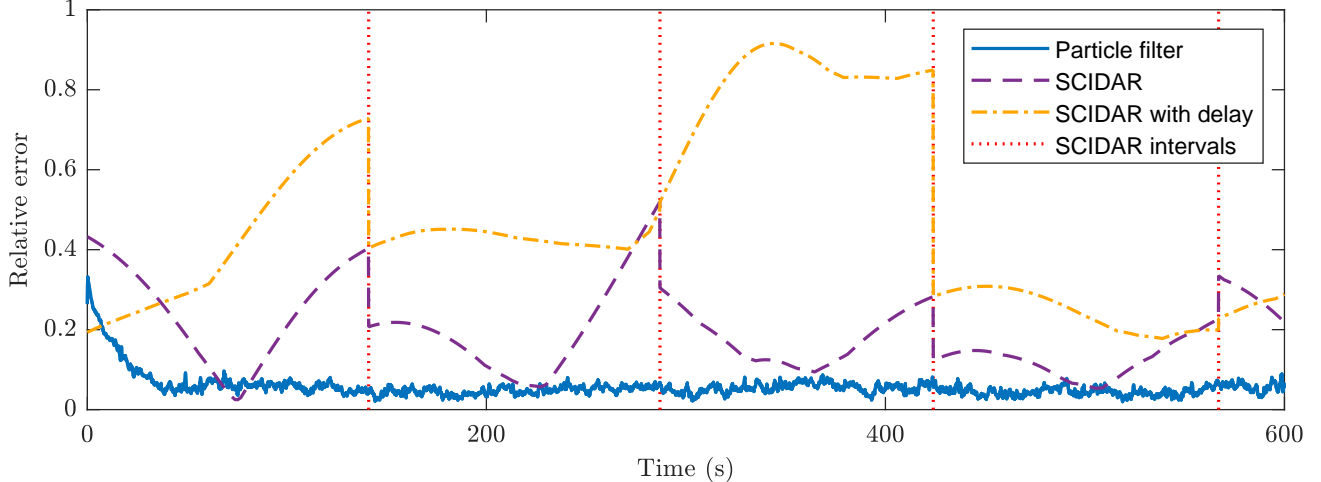
Figure 3. Relative error for the results shown in Fig. 2 (blue) and for the corresponding binned SCIDAR profiles. The error for SCIDAR is shown both using the profile corresponding to each time interval (purple), and using the profile from the previous time interval (yellow). The former shows the error caused by averaging over a long period of time, and the latter shows the actual error when using these profiles in an AO system, since the time delay is unavoidable in a real-world application. The vertical dotted red lines indicate the time intervals where each SCIDAR profile was measured.

In order to quantify the error in the obtained turbulence profiles, we define a relative error metric through

$$E_{C_n^2}(\boldsymbol{\rho}) = \frac{\sum_{k=1}^{K} |\rho_k - \rho_k^{\text{true}}|}{\sum_{k=1}^{K} \rho_k^{\text{true}}}, \tag{6}$$

where ρ_k^{true} is the simulated turbulence strength for the kth layer. Notice that with this particular error metric our purpose is merely to quantify the difference between profiles. Unfortunately, it is unclear how such an error metric is connected to tomographic error or AO system performance in general.

Fig. 3 shows the error as a function of time for the profiles shown in Fig. 2. We have also included the error given by the SCIDAR profiles for comparison. These profiles are constant in each interval indicated by the vertical dotted red lines, and since they were used to generate the simulated profile as described in Section 4, they perfectly match the average of the simulated profile in each time interval. We consider the error both when the SCIDAR profiles are used directly and when we introduce a delay by always using the profile from the previous time interval. The former is effectively a measure of the error caused by averaging the profile over the time interval, whereas the latter is the error that might be observed in practice, since the time delay is unavoidable in a real-time application.

The average error for the profiles given by the filter is 5.7 %. We can clearly see the effect of the random initialization with a wrong r_0, but after 20 to 30 seconds the error level seems to stabilize. Removing the first thirty seconds where the error is higher, we find that the long-term error level is 5.1 %. By contrast, we found that the SCIDAR profiles produce an error of 19.4 %, which increases to 46.5 % when we include the time delay. However, it is important to note that these errors are in no way specific to SCIDAR as a method, the errors arise purely from the limited temporal resolution which is an unavoidable feature of all commonly used turbulence profiling methods. Indeed, the fact that the simulated profiles were generated from SCIDAR data eliminates any possible error from the method itself, since these profiles are effectively treated as the ground truth.

Finally, we also considered the total turbulence strength of the profile, shown in Fig. 4. We found that the filter achieves an average relative error of just 1.1 %, whereas the error from using the SCIDAR profiles is 6.5 % without time delay and 25.2 % when the delay is included. We can also see that the total turbulence strength at the start is indeed 15 % higher than simulated, but it takes only 5 s for the filter to correct this error.
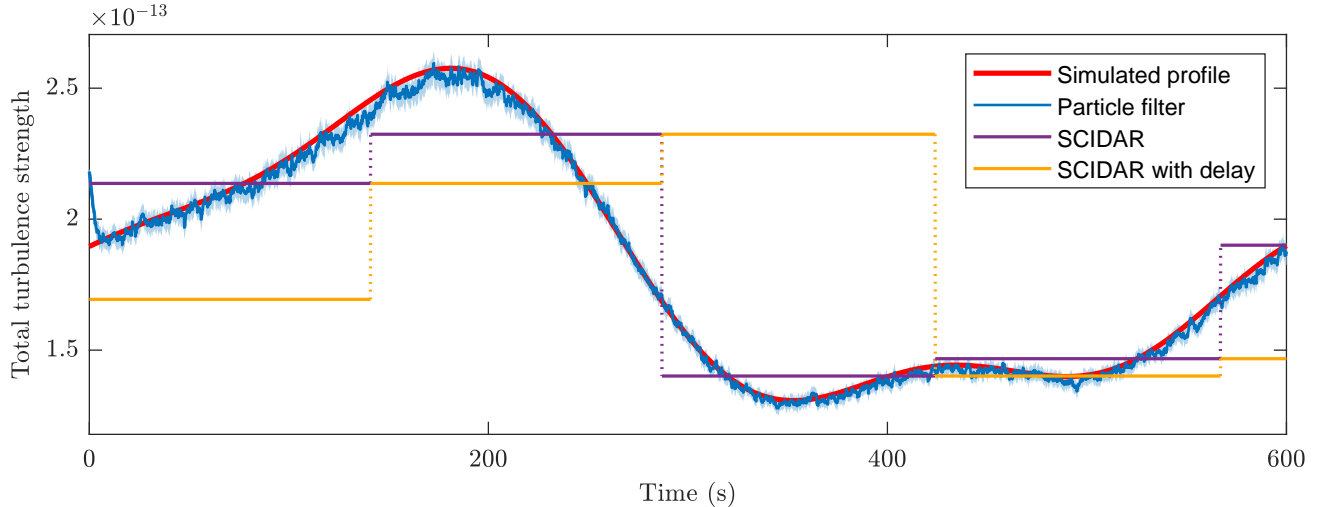
Figure 4. Total turbulence strength for the results shown in Fig. 2 (blue) and for the corresponding binned SCIDAR profiles (purple and yellow, as in Fig. 3). Similar to Fig. 2, we have also included a 95 % credible interval (light blue) around the mean of the filter, indicating the range in which the total turbulence strength falls with 95 % probability.

6. DISCUSSION

We have presented a novel method for real-time tracking of the turbulence profile, and applied it to ten minutes of simulated data from an ELT-scale telescope. The data was simulated with boiling phase screens using a time-dependent turbulence profile based on real profiles obtained with Stereo-SCIDAR at Paranal. Using this data, we have demonstrated that our method is capable of tracking significant changes in the turbulence profile and the average improvement over SCIDAR is substantial, when the unavoidable time delay in real scenarios is taken into account. Therefore, our method has the potential to improve tomographic reconstruction or point spread function estimation in AO systems by providing more accurate C_n^2-profiles. The results are also of interest for developing a clearer understanding of turbulence dynamics on shorter timescales.

Our future work includes expanding the numerical tests on the algorithm. Notice that the SCIDAR profiles picked for our simulations show larger variations than on average present in the data. Moreover, since no experimental data indicates how fast the fluctuations can be, the role of our simulated time-dependent profile is only indicative on what type of dynamics in the C_n^2-profile can be tracked. Furthermore, some steps could be taken to mitigate errors occurring in SCIDAR reconstructions in Section 5, such as using shorter time intervals for the profiles or, in the time-delayed case, updating the profiles more often. However, the filtering results can also be improved by using more computational resources, since we used significant dimension reduction on the data to reduce computational load, as described in Section 4. Finally, we plan to expand our numerical tests to real data in forthcoming articles.

ACKNOWLEDGMENTS

REFERENCES

[1] Tyson, R. K., [*Principles of Adaptive Optics*], CRC press (2015).

[2] Ellerbroek, B. L. and Vogel, C. R., "Inverse problems in astronomical adaptive optics," *Inverse Prob.* **25**(6), 063001 (2009).

[3] Ramlau, R., Saxenhuber, D., and Yudytskiy, M., "Iterative reconstruction methods in atmospheric tomography: FEWHA, Kaczmarz and Gradient-based algorithm," in [*SPIE Astronomical Telescopes+ Instrumentation*], *Proc. SPIE* **9148**, 91480Q (2014).

[4] Roddier, F., [*Adaptive Optics in Astronomy*], Cambridge University Press (1999).

[5] Helin, T., Kindermann, S., and Saxenhuber, D., "Towards analytical model optimization in atmospheric tomography," *Math. Methods Appl. Sci.* **40**(4), 1153–1169 (2017).

[6] Saxenhuber, D., Auzinger, G., Le Louarn, M., and Helin, T., "Comparison of methods for the reduction of reconstructed layers in atmospheric tomography," *Appl. Opt.* **56**(10), 2621–2629 (2017).

[7] Kornilov, V., Tokovinin, A., Shatsky, N., Voziakova, O., Potanin, S., and Safonov, B., "Combined MASS–DIMM instruments for atmospheric turbulence studies," *MNRAS* **382**(3), 1268–1278 (2007).

[8] Wilson, R. W., "SLODAR: measuring optical turbulence altitude with a Shack—Hartmann wavefront sensor," *MNRAS* **337**(1), 103–108 (2002).

[9] Butterley, T., Wilson, R. W., and Sarazin, M., "Determination of the profile of atmospheric optical turbulence strength from SLODAR data," *MNRAS* **369**(2), 835–845 (2006).

[10] Vernin, J. and Roddier, F., "Experimental determination of two-dimensional spatiotemporal power spectra of stellar light scintillation evidence for a multilayer structure of the air turbulence in the upper troposphere," *JOSA* **63**(3), 270–273 (1973).

[11] Shepherd, H., Osborn, J., Wilson, R., Butterley, T., Avila, R., Dhillon, V., and Morris, T., "Stereo-SCIDAR: optical turbulence profiling with high sensitivity using a modified SCIDAR instrument," *MNRAS* **437**(4), 3568–3577 (2013).

[12] Osborn, J. et al., "Optical turbulence profiling with Stereo-SCIDAR for VLT and ELT," *MNRAS* **478**(1), 825–834 (2018).

[13] Guesalaga, A., Neichel, B., Correia, C., Butterley, T., Osborn, J., Masciadri, E., Fusco, T., and Sauvage, J.-F., "Online estimation of the wavefront outer scale profile from adaptive optics telemetry," *MNRAS* **465**(2), 1984–1994 (2017).

[14] Lehtonen, J., Correia, C. M., and Helin, T., "Limits of turbulence and outer scale profiling with non-Kolmogorov statistics," in [*SPIE Astronomical Telescopes+ Instrumentation*], *Proc. SPIE* **10703**, 107036C (2018).

[15] Lehtonen, J. and Helin, T., "Correlation-based imaging in adaptive optics," in [*Mathematics in Imaging*], MW3D–3, Optical Society of America (2019).

[16] Helin, T., Kindermann, S., Lehtonen, J., and Ramlau, R., "Atmospheric turbulence profiling with unknown power spectral density," *Inverse Prob.* **34**(4), 044002 (2018).

[17] Law, K., Stuart, A., and Zygalakis, K., [*Data Assimilation: A Mathematical Introduction*], Springer (2015).

[18] Taylor, G. I., "The spectrum of turbulence," *Proc. R. Soc. Lond. A* , 476–490 (1938).

[19] Guesalaga, A., Neichel, B., Cortés, A., Béchet, C., and Guzmán, D., "Using the C_n^2 and wind profiler method with wide-field laser-guide-stars adaptive optics to quantify the frozen-flow decay," *MNRAS* **440**(3), 1925–1933 (2014).

[20] Srinath, S., Poyneer, L. A., Rudy, A. R., and Ammons, S. M., "Computationally efficient autoregressive method for generating phase screens with frozen flow and turbulence in optical simulations," *Opt. Express* **23**(26), 33335–33349 (2015).